Froehlich, K.; Ali, M.; Ramirez Hoyos, P.; Cervera Montesinos, J.; García-Morales, V.; Erdmann, M.; Ensinger, W. (2021). Effect of cationic polyamidoamine dendrimers on ionic transport through nanochannels. Electrochimica Acta. 367:1-8. https://doi.org/10.1016/j.electacta.2020.137263

Effect of cationic polyamidoamine dendrimers on ionic transport through nanochannels

Kristina Froehlich[a,*], Mubarak Ali[a,b], Patricio Ramirez[c], Javier Cervera[d], Vladimir García-Morales[d], Markus Erdmann, and Wolfgang Ensinger[a]

[a]*Dept. of Material- and Geo-Sciences, Materials Analysis, and Center of Synthetic Biology, Technische Universität Darmstadt, Alarich-Weiss-Str. 02, D-64287 Darmstadt, Germany*
[b]*Materials Research Department, GSI Helmholtzzentrum für Schwerionenforschung, Planckstrasse 1, D-64291, Darmstadt, Germany*
[c]*Dept. de Física Aplicada. Univ. Politècnica de València. E-46022 Valencia, Spain*
[d]*Dept. de Física de la Terra i Termodinàmica, Universitat de València, E-46100 Burjassot, Spain*

**Corresponding author. E-mail address: froehlich@ma.tu-darmstadt.de*

Abstract

The effect of polyamidoamine (PAMAM) dendrimers (generations G0-G3) on the current-voltage curves of conical and cylindrical nanochannels is studied either by surface functionalization or by addition to the electrolyte solution. Surface functionalization leads to inversion of the ion current rectification, indicating the anion selectivity of the modified nanochannels. This anion selectivity increases by immobilizing higher-generation dendrimers, as expected for an increase in the surface density of amino groups. However, compared to PAMAM G2, functionalization with PAMAM G3 results in higher cation and lower anion fluxes. Diffusion experiments of charged analytes across nanochannel membranes confirm the effects of the dendrimers. Our experimental and theoretical results show that the observed effects are independent of the nanochannel geometry, but primarily relate to the average charge density and distribution of fixed charges on the nanochannel surface.

Keywords: PAMAM dendrimer, ion current rectification, synthetic nanochannels, track-etching, surface functionalization

1. Introduction

Nanochannels belong to a new generation of devices designed for variety of potential application, e.g., sensing and molecular separation processes.[1–8] Fixed charges at the channel surface play an important role in ionic selectivity, and also in sensing process when the internal channel volume is of the order of the ionic analyte size. Nanochannels display ionic selectivity due to the attachment of charged groups to their surface. Thus, ions with opposite charge pass through the nanochannel, while the passage of coions is hindered.[6,9] Ionic selectivity can be increased when the surface potential is high and the channel radius is in the range of the Debye length of the electrolyte, typically on the nanometer scale.[10,11] In addition, the detection limit of a charged nanochannel sensor depends not only on the ion concentration in the electrolyte solution, but also on the charge density and distribution of fixed charges on the channel surface.[12,13]

The chemical modification of functional groups on the nanochannel walls allows to control the transport through them. A variety of different substrate-specific methods for surface modification has been reported.[14] By using these methods, it is possible to incorporate a diversity of functional groups onto the nanochannel surface, generating new sensory, transport and separation properties, for example in dependence of electrolyte pH value or temperature.[4,8,12,13,15]

A large variety of functional groups for nanochannel modification has been tailored for specific applications. Most of these were small molecules with little influence on the surface charge density. However, larger structures were also used for surface functionalization, for example proteins and polymers.[8,12,16,17] The deposition of polymer chains increases the charge density in nanochannels significantly. However, as far as we know, only linear and branched polymers have been used for nanochannel functionalization, depositing monolayer, brush and layer-by-layer assemblies to tailor the surface charges.

After a large number of successfully-linked linear functional groups on synthetic nanochannels, the next step is to modify the channel surface with higher branched, three-dimensional compounds. For this purpose, dendrimers are particularly suitable. Dendrimers are spherical, highly branched, nanoscale polymeric architectures with a very high density of surface groups. One of most studied dendrimers is polyamidoamine (PAMAM), composed of amidoamine monomer units, branching out from an ethylenediamine (EDA) core. Dendrimer

molecules of the same class are distributed by their generation (G). The addition of monomer units to the functional groups on the dendrimer surface create the next generation. In case of PAMAM with tertiary amino functional end groups, each additional generation results in doubling the number of amines on the molecule surface, starting from 4 (G0) to 8 (G1), 16 (G2) and 32 (G3). Due to their internal cavities capable of encapsulating guest molecules and the effective conjugation of various molecules to the surface functional groups, PAMAM dendrimers are used in different applications, such as drug delivery, gene therapy, and chemical separations.[18–21]

Uniformity at the molecular level and a high controllability of the molecular structure and properties make dendrimers highly attractive nanomaterials for application not only in solution, but also on solid surfaces as monolayer or multilayer dendrimer films. [22,23] The first example of covalent attachment of PAMAM dendrimers to a solid surface was reported by Crooks and coworkers, accomplished by the formation of amide bonds between the amino groups of the PAMAM dendrimer and the carboxylic acid groups of a self-assembled monolayer of mercaptoundecanoic acid on gold.[23] In other studies, dendritic compounds were deposited on glass or silicon surfaces or used to modify the surface properties of various polymeric substrates.[22,24] Other publications describe for example PAMAM G4 modified nanopipettes used for DNA sensing or the interaction between PAMAM G1 and the protein nanopore α-hemolysin.[21,25] Nevertheless, to the best of our knowledge, no studies of nanochannel functionalization by dendrimers have yet been reported.

We report the successful functionalization of conical and cylindrical nanopores with PAMAM dendrimers G0 to G3, and study their effect on the ion transport properties of the nanopores. The transport of ions and charged analytes through the modified nanochannels is investigated by measuring current-voltage curves and diffusion fluxes.[26]

2. Materials and methods

2.1 Materials

Ethylenediamine (EDA, 99.5%, Fluka), polyamidoamine (PAMAM) dendrimer kit generations G0-G3 (20 % weight fraction in methanol, Sigma-Aldrich), *N´*-(3-dimethylaminopropyl)-*N´*-

ethylcarbodiimide hydrochloride (EDC, ≥ 99%, Sigma-Aldrich) and pentafluorophenol (PFP, ≥ 99%, Sigma-Aldrich), potassium chloride (KCl, ≥ 99%, PanReac AppliChem), phosphate buffered saline (PBS, ≥ 99%, Sigma-Aldrich), disodium-1,5-naphthalenedisulfonic acid (NDS^{2-}, 85%, Fluka), methyl viologen dichloride hydrate (MV^{2+}, 98%, Sigma-Aldrich), sodium hydroxide (NaOH, 99%, Grüssing GmbH) and ethanol (≥ 99.8%, Roth) were used as received. All aqueous solutions were prepared in Milli-Q water (Millipore, resistance of > 18.2 M cm). The pH was adjusted with PBS buffer and measured with a bench pH meter (Phoenix Instrument GmbH).

2.2. Fabrication of ion track-etched nanochannel membranes

Polymer foil stacks of polyethylene terephthalate (PET, Hostaphan RN12) with a thickness of 12 µm were irradiated with swift heavy ions (Au^{25+}, energy: 11.4 MeV/u) at the universal linear accelerator (UNILAC) at GSI Helmholtz Center for Heavy Ion Research, Darmstadt (Germany).[27] To achieve single-ion irradiation, a metal mask with 200 µm diameter centered aperture was placed in front of the stacks. After a single ion passed through the stack, it was registered by a particle detector behind the samples and the ion beam was immediately blocked.

Cylindrical nanochannels were fabricated using symmetric track-etching technique.[9] The ion track-etched PET membranes were irradiated with UV light (Vilber Lourmat GmbH; VL-230.E, Lamp:T-30.M, maximum emission at 312 nm) for 1 h from each side. Then, the membranes were etched symmetrically by suspending them in a double-walled beaker filled with 2 M NaOH solution at 50 °C. Under these conditions, Nguyen *et al.* have reported an etching rate of around 5.4 nm/min. The membranes were etched for 20 min to achieve pore diameters of 100 nm. After etching, the membranes were washed with high purified water several times and stored in water overnight.

Conical-shaped nanochannels with typical radii around 600 nm – 750 nm at the base and 30 nm – 40 nm at the tip were fabricated using asymmetric track etching.[30] The PET membrane was placed between the chambers of a conductivity cell at 40 °C. One chamber was filled with 9 M NaOH solution and the other with a stopping solution of 1 M KCl and 1 M HCOOH. As soon as the channels open, the stopping solution neutralizes the etchant and

slows down further etching, thus generating conical-shaped nanochannels. During etching, a potential of −1 V was applied across the membrane and the current was monitored. The current remains zero while the channels are not open. After breakthrough, the current increases continuously. The etching was stopped at a certain current value corresponding to the desired tip diameter. After etching, the membranes were washed with stopping solution and high purified water several times and stored in water overnight to remove residual salts.

2.3. Surface functionalization of nanochannels

Heavy ion irradiation and the subsequent track-etching process generate carboxylic acid groups on the nanochannel surface. We used five functional amine molecules to modify these carboxylic acid groups: ethylenediamine (EDA) and the generations G0 to G3 of polyamidoamine (PAMAM) dendrimers. Their covalent linkage to the nanochannel surface was achieved through N-(3-(dimethylamino)propyl)-N'-ethylcarbodiimide/pentafluorophenol (EDC/PFP) coupling chemistry.[31] The chemical modification was performed with the PET membranes fixed in between the two chambers of a conductivity cell. The membranes with a single conical nanochannel were functionalized only from the tip side. The membranes with 10^7 cm^{-2} cylindrical nanochannels were functionalized symmetrically from both sides. In the activation step, the carboxylic acid groups were converted into reactive pentafluorophenyl esters by filling the chambers with ethanol solution containing 100 mM EDC and 200 mM PFP for 60 min. The chambers were then rinsed with ethanol to remove residues of EDC and PFP. Subsequently, the nanochannels were functionalized by filling the chambers with 1 mM (single-channel membrane) or 5 mM (10^7 cm^{-2} nanochannels) ethanolic solution of the corresponding amine molecules. To ensure complete immobilization, the functionalization was performed for at least 12 h overnight at room temperature. Finally, the functionalized nanochannel membranes were washed several times with ethanol and high purified water. They were stored in water before use.

2.4. Current-voltage (I-V) curves of single-nanochannel membranes

The single-nanochannel membrane was fixed in a conductivity cell before filling the chambers with KCl solution (in PBS buffer). A grounded (stainless steel) Faraday cage shield-

ed the cell from electrical interference. The electrodes were Ag/AgCl wires (1 mm diameter). The current-voltage (*I-V*) curves were measured using a Keithley 6487 picoamperemeter/voltage source (Keithley Instruments, Cleveland, OH, USA). A scanning triangular voltage, from +2 V to −2 V in 100 mV steps, was applied. Every data point was the average value of at least six individual measurements.

2.5. Theoretical modeling of the I-V curves

The *I-V* curves were modelled using the Poisson-Nernst-Planck equations. Assuming a conical geometry, the unknown model parameters were the tip radius α_L and the base radius α_R of the nanochannel and the surface charge density σ. The radius α_L was calculated from the slope of the linear *I-V* curve measured at low applied voltages in 1 M KCl solution under ambient conditions. The radius α_R and σ were determined by fitting the experimental data to the predictions to the theoretical model.[10,28,29]

2.6. Diffusion through membranes with 10^7 cm^{-2} *cylindrical nanochannels*

Methyl viologen (MV^{2+}) dichloride and disodium 1,5-naphthalene disulfonate (NDS^{2-}) were used as analytes in diffusion experiments across membranes containing 10^7 cm^{-2} cylindrical nanochannels (Figs. S4-S7).[17] A 25 mM solution of each analyte was prepared in 10 mM PBS buffer (pH 5.5 ± 0.1). The membrane was fixed between the chambers of the diffusion cell with a permeation area of 0.50 cm^2. One chamber (feed half-cell) was filled with 1.2 mL of the analyte solution and the other (permeate half-cell) with buffer solution. Inlet and outlet tubes (internal diameter 2.79 mm, length 38.1 cm, material Tygon LMT-55 (Hirschmann)) connect the permeate half-cell to an all-quartz flow-through cuvette (Suprasil®, Starna Scientific, volume 0.45 mL), which is placed in a UV/vis spectrophotometer (UV-3100PC, VWR International GmbH). The total volume of the permeate half-cell including tubes and cuvette is 6.3 mL. To generate a continuous flow through the cuvette and mixing of the permeate half-cell, the inlet tube is placed in a peristaltic pump (REGLO DIG MS-CA4/12, ColeParmer GmbH). The time resolution of the diffusion experiment is achieved by recording the absorbance signals with the "UV-Vis Analyst" software in "Wavelength Scan" mode. The wavelength range 200 nm – 350 nm is scanned in 1 nm steps and 30 s intervals.

3. Results and discussion

Before functionalization, the ion track-etched membranes containing conical or cylindrical nanochannels have carboxylic acid groups on the inner walls of the nanochannels. These are negatively charged under physiological conditions and, hence, unmodified nanochannels show cation selectivity. Functionalization of the nanochannel surfaces with ethylenediamine (EDA) and polyamidoamine (PAMAM) dendrimers creates a surface density of primary amino groups, as illustrated in Fig. 1. Since PAMAM dendrimers have an EDA core, we started with EDA (2 amino groups) and increased to 4, 8, 16 and 32 the number of primary amino groups per functional group using PAMAM G0, G1, G2 and G3 as surface modifiers. The experiments are carried out at pH 5.5 ± 0.1, using PBS buffer solution, so that all primary amino groups are expected to be protonated.[26] Hence, the modified nanochannels have positively-charged amino groups and show anion selectivity.

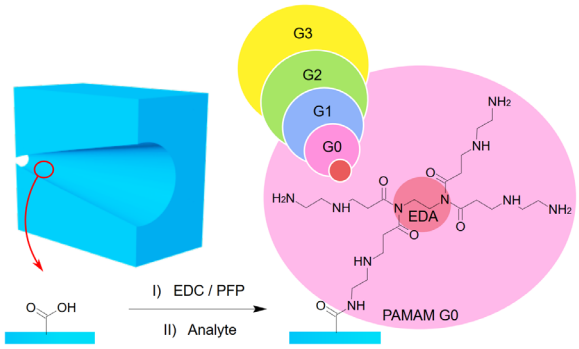

Fig. 1 Illustration of the functionalization of the carboxylic acid groups of a conical-shaped nanochannel with EDA and PAMAM dendrimers of generations G0 - G3. The increasing diameter of the colored circles represents increasing dendrimer size

3.1. I-V curves of single conical nanochannels

The effect of the EDA/PAMAM functionalization on the ion transport properties of the nanochannels was investigated by measuring their current-voltage (*I-V*) curves in 0.1 M KCl under ambient conditions, and comparing them with the curves of unmodified nanochannels. We used membranes with a single conical-shape nanochannel to avoid averaging of signals caused by multichannels and to achieve high sensitivity.

Unmodified nanochannels show cation selectivity. Anions are electrostatically hindered to enter the nanochannel and the current is mainly due to cations. Under positive potential ($V > 0$), cations are transported from the tip to the base of the conical nanochannel. Under negative potential ($V < 0$), cations flow in the opposite direction. The non-ohmic behavior is quantified by the current rectification ratio $r = |I(-2\ \mathrm{V})|/I(+2\ \mathrm{V})$.[28,30,32]

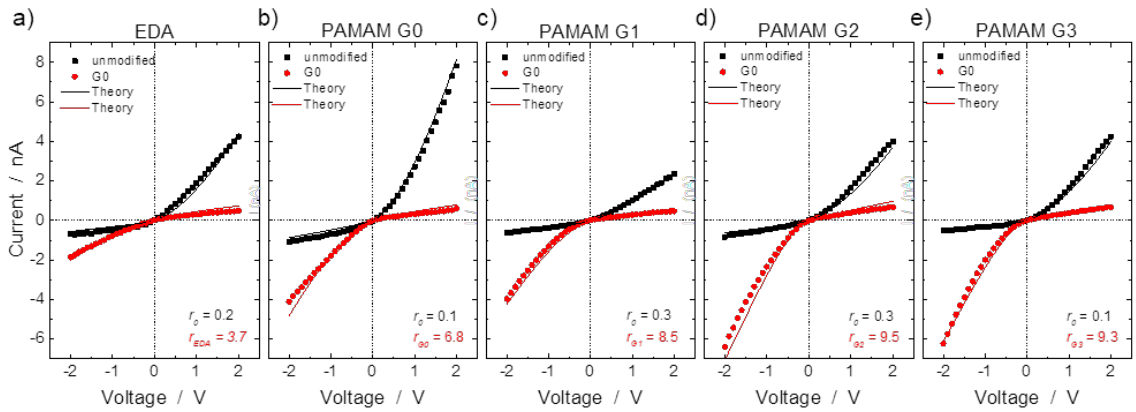

Fig. 2 Experimental (symbols) and calculated (lines) *I-V* curves of unmodified (black) and modified (red) conical nanochannels in 0.1 M KCl aqueous solution. Panels a-e correspond to modification with EDA and PAMAM dendrimers G0 – G3. The experimental rectification ratios of the same channel before (r_0) and after (r) modification are shown.

Modified nanochannels show anion selectivity. The functional groups differ in size and number of primary amino groups, having otherwise the same structure. The inversion of the surface charge density due to the functionalization leads to a reversal of the current rectification, so that $r > 1$ (Fig. 2). Increasing the surface charge density results in higher anion selectivity due to stronger electrostatic interactions between the ions and the positive surface functional groups. Thus, $r = 3.7$ for EDA-modified nanochannels, and r increases to 6.8, 8.5 and 9.5 for PAMAM G0, G1 and G2. The rectification ratio for PAMAM G3-modified nanochannels is r = 9.3, i.e., slightly smaller than for PAMAM G2. The steric hindrance of longer PAMAM chains may lead to a reduction of the surface charge density that explains this observation. The theoretical *I-V* curves in Fig. 2 are in good agreement with the experimental ones; the model parameters are shown in Table S1 in the supplementary information.

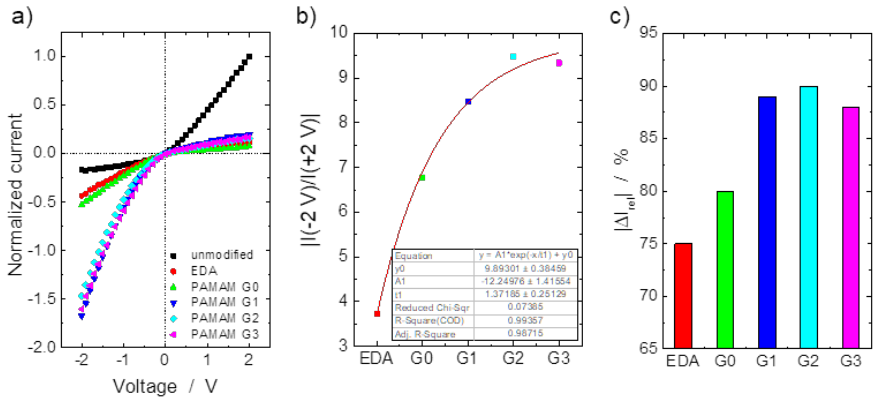

Fig. 3 (a) Experimental *I-V* curves of single conical nanochannels with currents normalized to $I_{\mathrm{before}}(-2\ \mathrm{V})$. b) The rectification ratio $r = |I(-2\ \mathrm{V})|/I(+2\ \mathrm{V})$ (b) and the relative increase $\Delta I_{\mathrm{rel}}(-2\ \mathrm{V})$ of the anionic current due to the surface functionalization (c) increase with the number of primary amino groups per functional group.

Slightly varying conditions during etching make each conical nanochannel unique. Hence, direct comparison of their *I-V* curves is not possible. Rather, the measured currents must be normalized using the current through the unmodified nanochannel at 2 V as a reference. That is, the normalized currents are calculated as

$$I^{\mathrm{n}}_{\mathrm{before}}(V) = \frac{I_{\mathrm{before}}(V)}{I_{\mathrm{before}}(+2\ \mathrm{V})/\mathrm{nA}}\ ,\quad I^{\mathrm{n}}_{\mathrm{after}}(V) = \frac{I_{\mathrm{after}}(V)}{I_{\mathrm{before}}(+2\ \mathrm{V})/\mathrm{nA}}\ , \tag{1}$$

where $I_{\mathrm{before}}(V)$ and $I_{\mathrm{after}}(V)$ are the measured currents at potential *V* before and after functionalization. Unmodified nanochannels have similar normalized *I-V* curves. Hence, only one is shown in Fig. 3a. The cation flow in the nanochannel is reduced from $I^{\mathrm{n}}_{\mathrm{before}}(+2\ \mathrm{V}) = 1\ \mathrm{nA}$ to approximately $I^{\mathrm{n}}_{\mathrm{after}}(+2\ \mathrm{V}) \approx 0.1\ \mathrm{nA}$ for EDA and PAMAM G0 and to $I^{\mathrm{n}}_{\mathrm{after}}(+2\ \mathrm{V}) \approx 0.2\ \mathrm{nA}$ for PAMAM G1, G2 and G3. Longer growing PAMAM chains create bigger cavities where cations can pass the channel with less electrostatic hindrance due to the same polarity, which could explain the small rise of PAMAM G2 and G3 compared to EDA and PAMAM G0. The current $I^{\mathrm{n}}_{\mathrm{after}}(-2\ \mathrm{V})$ due to the anions is 2.5 times larger than $I^{\mathrm{n}}_{\mathrm{before}}(-2\ \mathrm{V})$ in the case of EDA. The current $|I^{\mathrm{n}}_{\mathrm{after}}(-2\ \mathrm{V})|$ is due to the anions and increase with increasing number of primary amino groups per functional group. The values of $|I^{\mathrm{n}}_{\mathrm{after}}(-2\ \mathrm{V})|$ are 0.5 nA for EDA, 0.6 nA for PAMAM G0, 1.5 nA for G1, 1.8 nA for G2 and 1.7 nA for G3. On the one hand, the surface density of positively-charged amino groups increases and the anion selectivity increases. On the other hand, the growing size of the dendrimer deposited on the channel surface leads to steric repulsion of neighboring dendrimers. This steric hindrance

during and after surface functionalization results in a lower density of charged functional groups, which affects the anion selectivity.

The rectification ratio of the functionalized nanochannels increases the number of primary amino groups per functional group (Fig. 3b). In unmodified nanochannels with cation selectivity, the current $I_{\mathrm{before}}(-2\ \mathrm{V})$ is due mainly to cations flowing from base to tip. In modified nanochannels with anion selectivity, the current $I_{\mathrm{after}}(-2\ \mathrm{V})$ is due mainly to anions flowing from tip to base. The difference $I_{\mathrm{after}}(-2\ \mathrm{V}) - I_{\mathrm{before}}(-2\ \mathrm{V})$ can be attributed to the anion transport due to the nanochannel functionalization. The relative increase after functionalization of the current at −2 V

$$\Delta I_{\mathrm{rel}}(-2\ \mathrm{V}) = \frac{I_{\mathrm{after}}(-2\ \mathrm{V}) - I_{\mathrm{before}}(-2\ \mathrm{V})}{I_{\mathrm{after}}(-2\ \mathrm{V})} \quad (2)$$

can be interpreted as the fraction of the current due mainly to anions. The quantity $\Delta I_{\mathrm{rel}}(-2\ \mathrm{V})$ also increases the number of primary amino groups per functional group (Fig. 3c). Functionalization with EDA produces $\Delta I_{\mathrm{rel}}(-2\ \mathrm{V}) = 75\%$. This quantity increases to $\Delta I_{\mathrm{rel}}(-2\ \mathrm{V}) = 80\%$ for PAMAM G0 and reaches a maximum $\Delta I_{\mathrm{rel}}(-2\ \mathrm{V}) = 90\%$ for PAMAM G2. For PAMAM G3, $\Delta I_{\mathrm{rel}}(-2\ \mathrm{V})$ is slightly smaller than for PAMAM G2 which, as mentioned before, can be due to a reduction of the surface charge density in the case of higher generation dendrimers because of steric hindrance.

3.2. Physical adsorption of dendrimers

To study the effect of the physical adsorption of dendrimers on the ion transport properties of the unmodified, single conical nanochannels, we have measured their *I-V* curves in mixed solutions containing 0.1 M KCl and PAMAM dendrimers in concentrations ranging from 1 nM to 1 mM. The unmodified nanochannels have cation selectivity and the dendrimers are positively charged, so that their physical adsorption could be expected to reduce the cation selectivity or generate anion selectivity.

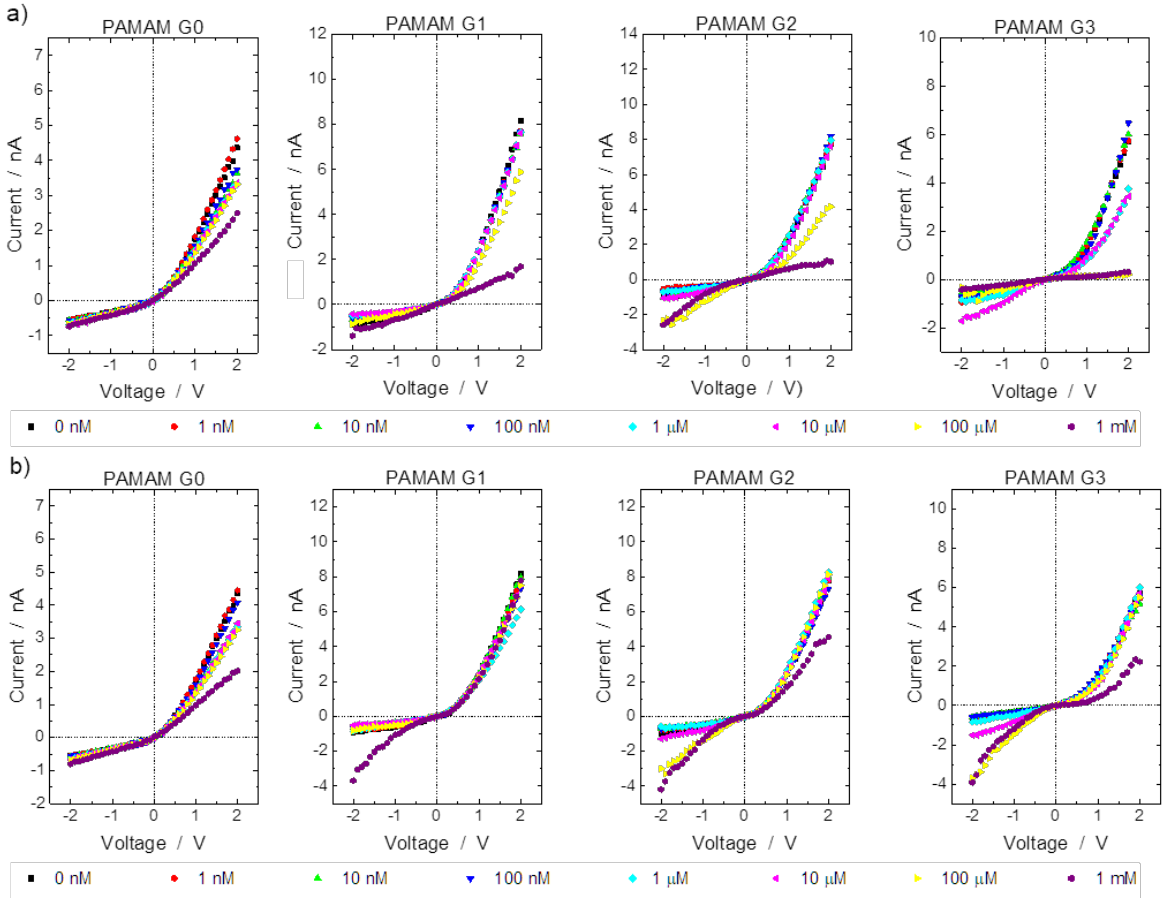

Fig. 4 *I-V* curves of unmodified, single conical nanochannels in mixed solutions of 0.1 M KCl and varying concentrations of PAMAM dendrimers. (a) Under symmetrical conditions, both nanochannels chambers contain the same solution. (b) Under asymmetric conditions, the solution in contact with the tip contains KCl and PAMAM dendrimers and the solution in contact with the base only contains KCl.

Under symmetrical electrolyte conditions, both sides of the nanochannel are exposed to the KCl+dendrimer solution (Fig. 4a). A reduction in the cation selectivity with increasing PAMAM concentration is then observed for all dendrimer generations. The current $I(2\ \mathrm{V})$ decreases with increasing concentration of PAMAM G0. Its value for 1 mM is approximately half of that in absence of PAMAM G0. PAMAM G1 and G2 concentrations below $100\ \mu\mathrm{M}$ do not affect $I(2\ \mathrm{V})$. The reduction of $I(2\ \mathrm{V})$ is around 25% for $100\ \mu\mathrm{M}$ PAMAM G1 and around 50% for $100\ \mu\mathrm{M}$ PAMAM G2. PAMAM G3 concentrations below $1\ \mu\mathrm{M}$ do not affect $I(2\ \mathrm{V})$. The reduction of $I(2\ \mathrm{V})$ is around 65% for $1\ \mu\mathrm{M}$ PAMAM G3. Concentrations of PAMAM G3 higher than $10\ \mu\mathrm{M}$ cause a reduction of both $I(2\ \mathrm{V})$ and $|I(-2\ \mathrm{V})|$, which may indicate that their physical adsorption on the nanochannel surface blocks the nanochannel openings or causes steric hindrance effects. The effect of dissolved PAMAM G0 on $I(-2\ \mathrm{V})$ is negligible at all concentrations. The current $|I(-2\ \mathrm{V})|$ increases with increasing concentration of PA-

MAM G1. For 1 mM PAMAM G2, the *I-V* curve shows an inversion of the rectification. In particular, the rectification ratio is $r = |I(-2\ \mathrm{V})|/I(+2\ \mathrm{V}) = 2.5$, which indicates a polarity reversal of the surface charges due to physical adsorption of the dendrimers on the nanochannel surface. In case of PAMAM G3, $|I(-2\ \mathrm{V})|$ is maximum for $10\ \mu\mathrm{M}$ dendrimer concentration, with an increase of almost 150% with respect to absence of PAMAM G3 in solution. However, there is no rectification inversion and $r = |I(-2\ \mathrm{V})|/I(+2\ \mathrm{V}) < 1$.

Under asymmetrical conditions, the tip of conical nanochannel is exposed to the KCl+dendrimer solution and its base is in contact with 0.1 M KCl (Fig. 4b). Generally speaking, the effect of the dendrimer in solution is smaller on $I(+2\ \mathrm{V})$ than on $I(-2\ \mathrm{V})$. The reduction of $I(+2\ \mathrm{V})$ due to PAMAM G0 is significant for $10\ \mu\mathrm{M}$ and larger concentrations. PAMAM G1 does not have any influence on $I(V)$ for $V > 0$. The effect of PAMAM G2 and G3 on $I(V)$ for $V > 0$ is noticeable only at 1 mM. On the contrary, PAMAM G1 and G2 significantly increase $|I(V)|$ for $V < 0$. PAMAM G0 shows no significant influence on $I(-2\ \mathrm{V})$. The shape of the *I-V* curve changes from the typical diode-like to a "S"-shaped (with lower conductance at lower absolute values of the voltage) in the presence of PAMAM G1 (1 mM), G2 ($100\ \mu\mathrm{M}$) and G3 ($100\ \mu\mathrm{M}$). This curve shape indicates the physical adsorption of dendrimers on the nanochannel tip, resulting in positively-charged functional groups on the nanochannel surface, while the base of the conical nanochannel is still negatively charged (Fig. S1)

Under symmetric and asymmetric conditions, the rectification ratio increases with increasing dendrimer concentration and dendrimer generation (Fig. S2).

3.3. Diffusion through membranes with 10^7 cm^{-2} *functionalized nanochannels*

Analyte permeation experiments for characterization of track-etched membranes often use manual sample collection.[33] In this work, we performed pseudo-automated mass transport experiments using a setup described by Duznovic *et al*.[17] Automated measurements of mass transport prevent errors coming from manual handling, volume loss resulting dilution errors and permit the detection of signal changes in UV/vis measurements in very short time scales allowing a very precise determination of analyte diffusion rates.

In our setup the permeate cell was connected to the flux-cell cuvette placed in the detection chamber of a UV/vis spectrophotometer. The time-resolved detection of the ana-

lyte permeation was achieved by the interposition of a peristaltic pump to obtain a constant circulation of permeate solution. The transport measurements are collected in adjustable time steps by starting the UV/vis detection manually using a stop watch.

In the first step, the calibration curve for known organic analyte concentrations was recorded (Figs. S3a and b). For the calibration of positively charged methyl-viologen (MV^{2+}) and negatively charged 1,5-naphthalene disulfonate (NDS^{2-}) maximum absorbance is obtained at a wavelength (λ_{max}) of 257 nm and 288 nm. Using Lambert-Beer's equation, unknown analyte concentration in the permeate solution can be determined from the calibration curve (Fig. S3c).

Diffusion experiments through membranes having 10^7 cm^{-2} cylindrical nanochannels, with a diameter around 100 nm, were performed before and after their functionalization with PAMAM dendrimers. Each functionalization was performed at least three times to ensure the reliability of its effect on the transport of charged analytes. For analysis, we used data from measurements with the least fluctuations. Using the linear equation from the calibration curve and absorbance at λ_{max} of MV^{2+} and NDS^{2-} for each diffusion step, the analyte permeation rate was calculated from the linear regression of their slope. The UV/vis spectra and the linear regressions of the analyte permeation rate are presented in Figs. S4-S7.

The UV/vis spectra in Figs. 5a and b after 6 min of diffusion of MV^{2+} and NDS^{2-} show the change in the signal intensity caused by surface functionalization with PAMAM G3. This change is used to evaluate the diffusion flux. For short diffusion times the concentration difference between feed and permeation cells is approximately constant. The time-resolved permeation shows a linear dependence with time of the amount of analyte that has diffused through the membrane, as expected from Fick's law (Fig. 5c). Diffusion times beyond 10 min should not be used because the UV/vis spectra of MV^{2+} through unmodified nanochannels then give signal intensities above 2 and reach the limit of applicability of the Lambert-Beer law.

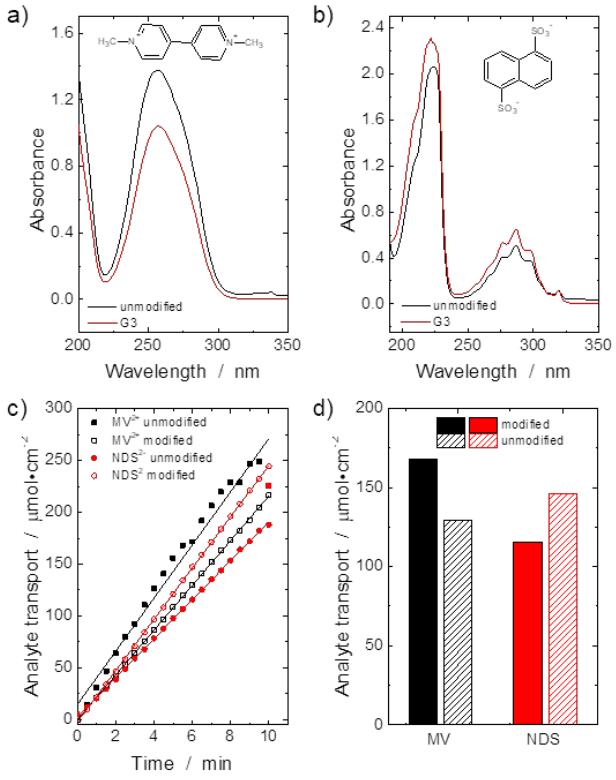

Fig. 5 Effect of functionalization with PAMAM G3 on the diffusion fluxes of charged MV^{2+} and NDS^{2-} through membranes having 10^7 cm^{-2} cylindrical nanochannels compared to unmodified nanochannels. UV/vis absorption spectra of a) MV^{2+} and b) NDS^{2-} after 6 min of diffusion. c) Amounts of MV^{2+} and NDS^{2-} that have diffused across the membranes as a function of time. d) Comparison of amounts of analyte transported during 6 min of diffusion before and after modification.

The diffusion flux of MV^{2+} through unmodified nanochannels is $0.468\ \mu mol\ cm^{-2}\ s^{-1}$ and decreases to $0.359\ \mu mol\ cm^{-2}\ s^{-1}$ after nanochannel functionalization with PAMAM G3. This reduction is in agreement with the well-known fact that the diffusion coefficient of an electrolyte, such as $(MV)Cl_2$, through a charged nanochannel is approximately that of the co-ion. In the case of unmodified nanochannels with cation selectivity the coion is Cl^- and in the case of functionalized nanochannels with anion selectivity the coion is MV^{2+}. Since MV^{2+} has a smaller diffusion coefficient than Cl^-, the diffusion flux of $(MV)Cl_2$ should be smaller through the anion-selective, functionalized nanochannel, in agreement with experimental observations. Consistently, for an electrolyte, such as $Na_2(NDS)$, the coion is NDS^{2-} in the case of unmodified nanochannels and the coion is Na^+ in the case of functionalized nanochannels. Since Na^+ has a larger diffusion coefficient than NDS^{2-}, the diffusion flux of $Na_2(NDS)$ should be larger through the anion-selective, functionalized nanochannel than through the unmodified nanochannel. Experimental observations agree with this prediction:

the diffusion flux of NDS^{2-} increases from $0.321\ \mu mol\ cm^{-2}\ s^{-1}$ to $0.406\ \mu mol\ cm^{-2}\ s^{-1}$ after functionalization with PAMAM G3 (Fig. 5d).

In order to compare the effects of the different functionalizations, we set a benchmark of 6 min diffusion time and calculated the ratios of the flux through functionalized membranes and the flux through the unmodified membrane (Fig. 6). In the case of the positively-charged analyte (MV^{2+}), these diffusion flux ratios are 0.64 for G0, 0.46 for G1, 0.38 for G2 and 0.77 for G3. In the case of the negatively-charged analyte (NDS^{2-}), the diffusion flux ratios are 1.27 for G0, 1.72 for G1, 2.07 for G2 and 1.27 for G3. All these results agree with the prediction that a surface functionalization that changes unmodified, cation-selective nanochannels into anion-selective nanochannels lead to a decrease of the diffusion coefficient of $(MV)Cl_2$ and to an increase of the diffusion coefficient of $Na_2(NDS)$ through the nanochannels.

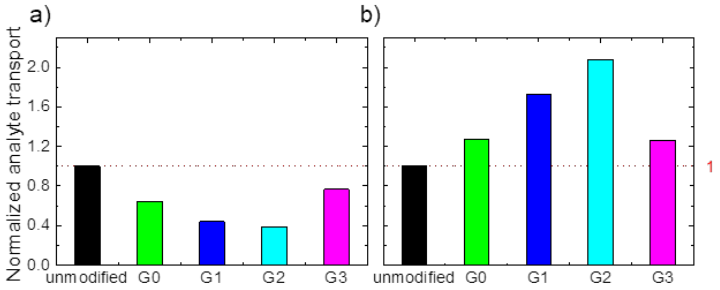

Fig. 6 Diffusion fluxes, normalized to the flux through the unmodified membrane, of a) MV^{2+} dichloride and b) disodium NDS^{2-} through membranes with 10^7 cm^{-2} cylindrical nanochannels after modification with PAMAM dendrimers G0-G3. The fuxes have been evaluated from the observed concentration changes after 6 min diffusion.

These results agree with our previous conclusions drawn from the measured *I-V* curves (Fig. 3): the positive surface charge density on the functionalized nanochannels increases with the PAMAM dendrimer generation number for G0, G1 and G2, as expected from the increased number of primary amino groups per functional group. However, the surface charge density of the nanochannels functionalized with PAMAM G3 is smaller than that of the nanochannels functionalized with PAMAM G2. In fact, PAMAM G0 and G3 have quite similar effects on the diffusion fluxes of $(MV)Cl_2$ and $Na_2(NDS)$ (Fig. 6).

Since the nanochannels used in the diffusion experiments and in the I-V measurements differ in shape and channel diameter, we conclude that the effects of PAMAM den-

drimers is independent of the nanochannel geometry. Instead, the ion transport properties of the functionalized nanochannels is sensitive to the size and geometry of the deposited dendrimer, which mainly determine the charge density on the nanochannel surfaces.

4. Conclusion

We fabricated conical and cylindrical shaped nanochannels and functionalized their surfaces with PAMAM dendrimers (generations G0 to G3). The experimental results clearly showed that the functionalization with dendrimers reduces the cation fluxes and increase the anion fluxes across the nanochannels. PAMAM G3 has weaker effects on the ion transport than PAMAM G2. In case of conical-shaped nanochannels the ion fluxes after G3 deposition are comparable with G1 and G2, and in the case of cylindrical nanochannels they are comparable with G0. The effect of the functionalization with PAMAM dendrimers is independent of the nanochannel shape and diameter. Hence, it is possible to control ion current/mass transport not only by changing surface polarity or channel diameter during the chemical modification process, but also by changing the surface charge density and distribution of PAMAM dendrimers of different generations. These results give new insights into the importance of the density and distribution of fixed charges on nanoscale surface materials. The functionalization of nanochannel devices with dendrimers opens opportunities in sensor, separation, and storage applications.

Acknowledgements

The authors acknowledge the support from the LOEWE project iNAPO, Hessen State Ministry of Higher Education, Research and the Arts, Germany and from project PGC2018-097359-B-I00, Ministry of Science and Innovation, Spain, and FEDER. Helpful discussions with Prof. Salvador Mafe are acknowledged. Special thanks to Prof. C. Trautmann and Dr. E. Toimil Molares (GSI, Material Research Department) for their support with the heavy ion irradiation experiments. The heavy ion irradiation is based on a UMAT experiment, which was performed at the X0-beamline of the UNILAC at the GSI Helmholtzzentrum fuer Schwerionenforschung, Darmstadt (Germany) in the frame of FAIR Phase-0.

References

[1] S. Lee, Y. Zhang, H. S. White, C. C. Harrell, C. R. Martin, *Analytical chemistry* **2004**, *76*, 6108.

[2] M. Ali, B. Yameen, R. Neumann, W. Ensinger, W. Knoll, O. Azzaroni, *Journal of the American Chemical Society* **2008**, *130*, 16351.

[3] R. B. Schoch, J. Han, P. Renaud, *Rev. Mod. Phys.* **2008**, *80*, 839.

[4] M. Ali, P. Ramirez, S. Mafé, R. Neumann, W. Ensinger, *ACS nano* **2009**, *3*, 603.

[5] M. Ali, P. Ramirez, I. Duznovic, S. Nasir, S. Mafe, W. Ensinger, *Colloids and surfaces. B, Biointerfaces* **2017**, *150*, 201.

[6] S. Nasir, M. Ali, J. Cervera, V. Gomez, M. Hamza Ali Haider, W. Ensinger, S. Mafe, P. Ramirez, *Journal of colloid and interface science* **2019**, *553*, 639.

[7] M. Ali, I. Ahmed, P. Ramirez, S. Nasir, S. Mafe, C. M. Niemeyer, W. Ensinger, *Analytical chemistry* **2018**, *90*, 6820.

[8] L. K. Müller, I. Duznovic, D. Tietze, W. Weber, M. Ali, V. Stein, W. Ensinger, A. Tietze, *Chemistry (Weinheim an der Bergstrasse, Germany)* **2020**.

[9] Q. H. Nguyen, M. Ali, V. Bayer, R. Neumann, W. Ensinger, *Nanotechnology* **2010**, *21*, 365701.

[10] J. Cervera, B. Schiedt, R. Neumann, S. Mafé, P. Ramírez, *The Journal of chemical physics* **2006**, *124*, 104706.

[11] S. Mafe, J. A. Manzanares, J. Pellicer, *J. Membr. Sci.* **1990**, *51*, 161.

[12] B. Yameen, M. Ali, R. Neumann, W. Ensinger, W. Knoll, O. Azzaroni, *Journal of the American Chemical Society* **2009**, *131*, 2070.

[13] L. Wang, W. Guo, Y. B. Xie, X. W. Wang, J. M. Xue, Y. G. Wang, *Radiation Measurements* **2009**, *44*, 1119.

[14] M. Lepoitevin, T. Ma, M. Bechelany, J.-M. Janot, S. Balme, *Advances in colloid and interface science* **2017**, *250*, 195.

[15] a) W. Guo, H. Xia, L. Cao, F. Xia, S. Wang, G. Zhang, Y. Song, Y. Wang, L. Jiang, D. Zhu, *Adv. Funct. Mater.* **2010**, *20*, 3561; b) B. Yameen, M. Ali, R. Neumann, W. Ensinger, W. Knoll, O. Azzaroni, *Small (Weinheim an der Bergstrasse, Germany)* **2009**, *5*, 1287.

[16] M. Ali, B. Yameen, J. Cervera, P. Ramírez, R. Neumann, W. Ensinger, W. Knoll, O. Azzaroni, *Journal of the American Chemical Society* **2010**, *132*, 8338.

[17] I. Duznovic, M. Diefenbach, M. Ali, T. Stein, M. Biesalski, W. Ensinger, *Journal of Membrane Science* **2019**, *591*, 117344.

[18] B. Devarakonda, R. A. Hill, M. M. de Villiers, *International journal of pharmaceutics* **2004**, *284*, 133.

[19] W.-P. Zhu, J. Gao, S.-P. Sun, S. Zhang, T.-S. Chung, *Journal of Membrane Science* **2015**, *487*, 117.

[20] U. Gupta, O. Perumal in *Natural and Synthetic Biomedical Polymers*, Elsevier, **2014**, pp. 243–257.

[21] Y. Fu, H. Tokuhisa, L. A. Baker, *Chemical communications (Cambridge, England)* **2009**, 4877.

[22] D. C. Tully, J. M. J. Fréchet, *Chem. Commun.* **2001**, 1229.

[23] R. M. Crooks and A. J. Ricco, *Acc. Chem. Res.* **1998**, *31*, 219.

[24] A. El Kadib, N. Katir, M. Bousmina, J. P. Majoral, *New J. Chem.* **2012**, *36*, 241.

[25] A. Asandei, A. Ciuca, A. Apetrei, I. Schiopu, L. Mereuta, C. H. Seo, Y. Park, T. Luchian, *Scientific reports* **2017**, *7*, 6167.

[26] P. K. Maiti, T. Çağın, S.-T. Lin, W. A. Goddard, *Macromolecules* **2005**, *38*, 979.

[27] T. W. Cornelius, P.Y. Apel, B. Schiedt, C. Trautmann, M. E. Toimil-Molares, S. Karim, R. Neumann, *Nuclear Instruments and Methods in Physics Research Section B: Beam Interactions with Materials and Atoms* **2007**, *265*, 553.

[28] M. Ali, P. Ramirez, S. Mafe, R. Neumann, W. Ensinger, *ACS nano* **2009**, *3*, 603.

[29] J. Cervera, B. Schiedt, P. Ramírez, *Europhys. Lett.* **2005**, *71*, 35.

[30] P. Y. Apel, Y. E. Korchev, Z. Siwy, R. Spohr, M. Yoshida, *Nucl. Instrum. Methods Phys. Res., Sect. B* **2001**, *184*, 337.
[31] M. Ali, S. Nasir, P. Ramirez, J. Cervera, S. Mafe, W. Ensinger, *J. Phys. Chem. C* **2013**, *117*, 18234.
[32] Y. Tian, Z. Zhang, L. Wen, J. Ma, *Chemical communications (Cambridge, England)* **2013**, *49*, 10679.
[33] a) Q. H. Nguyen, M. Ali, S. Nasir, W. Ensinger, *Nanotechnology* **2015**, *26*, 485502; b) S. E. Létant, C. M. Schaldach, M. R. Johnson, A. Sawvel, W. L. Bourcier, W. D. Wilson, *Small (Weinheim an der Bergstrasse, Germany)* **2006**, *2*, 1504; c) Rostovtseva, T. et al.